Nanometer thick single crystal Y_2O_3 films epitaxially grown on Si (111) with structures approaching perfection

C. W. Nieh,[1] Y. J. Lee,[1] W. C. Lee,[1] Z. K. Yang,[1] A. R. Kortan,[1,a)] M. Hong,[1,b)] J. Kwo,[2] and C.-H. Hsu[3,c)]
[1]*Department of Materials Science and Engineering, National Tsing Hua University, Hsinchu, Taiwan 30013, Taiwan*
[2]*Department of Physics, National Tsing Hua University, Hsinchu, Taiwan 30013, Taiwan*
[3]*National Synchrotron Radiation Research Center, Hsinchu, Taiwan 30076, Taiwan*

(Received 21 November 2007; accepted 23 January 2008; published online 15 February 2008)

Cubic phase Y_2O_3 films 1.6–10 nm thick of excellent quality have been epitaxially grown on Si (111) with $Y_2O_3(111)\|Si(111)$ using electron beam evaporation of Y_2O_3 in ultrahigh vacuum. Structural and morphological studies were carried out by x-ray scattering and reflectivity and high-resolution transmission electron microscopy, with the growth being *in situ* monitored by reflection high energy electron diffraction. There are two Y_2O_3 domains in the initial stage of the oxide growth with equal population, and the *B*-type domain of $Y_2O_3[2\bar{1}\bar{1}]\|Si[11\bar{2}]$ becomes predominating over the *A*-type domain of $Y_2O_3[2\bar{1}\bar{1}]\|Si[2\bar{1}\bar{1}]$ with increasing film thickness. Besides the excellent crystallinity of the films as derived from the small ω-rocking curve width of 0.014°, our results also show atomically sharp smooth surface and interfaces. © *2008 American Institute of Physics*. [DOI: 10.1063/1.2883939]

Y_2O_3/Si heterostructure has long been a subject of scientific and technological interest. Y_2O_3 is attractive as an alternative gate dielectric based on its high dielectric constant, high conduction band offset, and thermodynamic stability with Si.[1,2] Moreover, a small lattice mismatch of −2.4% between Si $[2\times a(\mathrm{Si})=1.086\ \mathrm{nm}]$ and cubic phase Y_2O_3 $[(a(Y_2O_3)\ =1.060\ \mathrm{nm}]$ has led many attempts to grow epitaxial Y_2O_3 films on Si, which may serve as templates for overgrowing Si and other semiconductors [e.g., GaN Ref. 3] for applications such as silicon on insulator,[4] three-dimensional integrated circuit, and integration of photonic devices with Si electronic circuits.

Y_2O_3 (110) was found to epitaxially grow on Si (100) with two degenerated domains of equal population.[2,5,6] The employment of vicinal (001) Si substrates of 4° miscut along $[1\bar{1}0]$ has resulted in the growth of mostly single-domain (110) orientated epitaxial films with the alignment of in-plane axes of $Y_2O_3[001]\|Si[110]$ and $Y_2O_3[1\bar{1}0]\|Si[1\bar{1}0]$. A low electrical leakage current density was obtained due to the elimination of domain boundaries.[2,5] The growth of Y_2O_3 (110) on Si (100), rather than Y_2O_3 (100), is perhaps caused by the minimum-energy requirement. Efforts were also taken to grow single-crystal Y_2O_3 on Si (111) substrates, expecting to grow Y_2O_3 (111) in parallel with that of Si.[7,8] It was found, however, that despite a smaller in-plane lattice mismatch it has been difficult to achieve a good epitaxial Y_2O_3 layer of less than 5–10 nm on Si (111). The difficulty in achieving good oxide crystal in the nanometer regime, namely in the initial growth, has been attributed to the oxide film deposition technique.

Our previous work of growing Sc_2O_3 on Si (111) with electron beam evaporation from an oxide source in ultrahigh vacuum[9] (UHV) has resulted in achieving epitaxial nanometer thick single crystal with excellent crystallinity despite a lattice mismatch of −9.2% between Si and cubic phase Sc_2O_3 $[a(Sc_2O_3)=0.986\ \mathrm{nm}]$.[10] The ω-rocking curves of Sc_2O_3 (3.4 nm thick) (222) and (444) peaks reveal full width at half maximum (FWHM) values of 0.033° and 0.044°, respectively. With a smaller lattice mismatch in Y_2O_3/Si, it was expected to attain nanometer-thick Y_2O_3 with better film quality. Indeed, in this letter, excellent growth of nanometer-thick Y_2O_3 (111) films on Si (111) has been achieved. The oxide films were deposited using electron beam evaporation of a powder-packed Y_2O_3 target in UHV. X-ray scattering and reflectivity using synchrotron radiation and high-resolution transmission electron microscopy (HR-TEM) were used to study the Y_2O_3/Si (111) heteroepitaxial system.

The cleaning and hydrogen passivation of Si (111) wafers and the Si surface preparation for the subsequent oxide growth were described in Ref. 10. The thin Y_2O_3 films were then deposited on the reconstructed Si surface, with substrate temperatures maintaining at about 780 °C. Sharp (4×4) patterns were observed after the growth of Y_2O_3 film ~3 nm thick, indicating high crystalline quality of the films with atomically smooth surface. After deposition, the samples were capped with a thin layer of Si for protection. HR-TEM specimens were prepared with mechanical polishing, dimpling, and ion milling using a Gatan precision ion polishing system operated at 3 kV. HR-TEM images were taken using a field-emission gun type TEM (JEM-2100F) operated at 200 kV. The synchrotron x-ray measurements were performed at wiggler beamline BL17B1 at the National Synchrotron Radiation Research Center (NSRRC), Taiwan, and the detailed experiment was described in Ref. 11. High-resolution x-ray measurements were carried out in single-crystal geometry. X-ray reflectivity measurement was per-

a)Now at: the Department of Energy, USA.
b)Author to whom correspondence should be addressed. Electronic mail: mhong@mx.nhtv.edv.tw.
c)Author to whom correspondence should be addressed. Also at: Department of Photonics, National Chiao Tung University, Hsinchu, 30010, Taiwan. Electronic mail: chsu@nsrrc.org.tw.

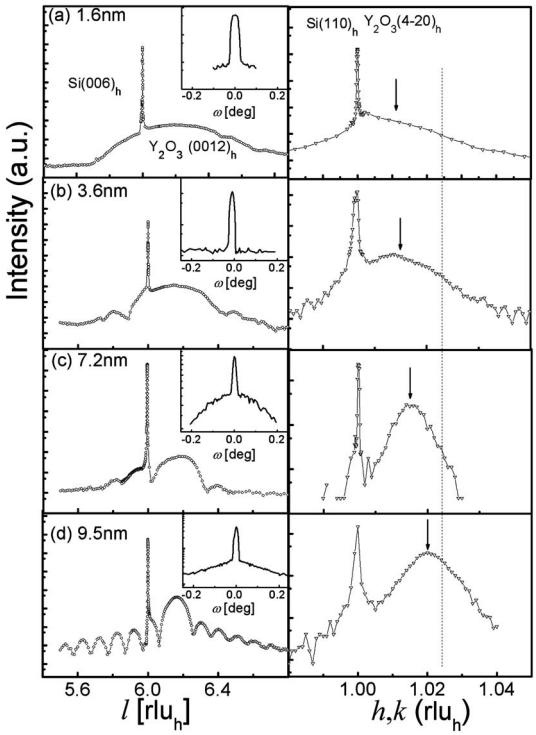

FIG. 1. The radial scans along surface normal, i.e., along $(00l)_h$ (left panel) and lateral $(110)_h$ direction (right panel). The position of Y_2O_3 $(4\bar{2}0)$ surface reflections are marked by arrows. The ω rocking curves (insets) of (a) 1.6, (b) 3.6, (c) 7.2, and (d) 9.5 nm thick Y_2O_3 layers, with the FWHM values of 0.033, 0.017, 0.014, and 0.014°, respectively. The *y*-axis is in a logarithmic scale.

formed to determine the film thickness and the surface/interfacial roughness.[12]

To conveniently decouple the normal and in-plane components of momentum transfer in x-ray scattering measurements, a hexagonal unit cell (h) was adapted by coordinate transformation from commonly used cubic unit cell. In reciprocal space, the basis vectors are transformed following $(100)_h=(4\bar{2}\bar{2})/3$, $(010)_h=(22\bar{4})/3$, and $(001)_h=(111)/3$, where the momentum transfer in the direction normal to the interface is represented by a single index l.[13] The left panel of Fig. 1 illustrates the scattered x-ray intensity distribution along Si $(006)_h$ crystal truncation rods of four samples with different oxide thicknesses of 1.6, 3.6, 7.2, and 9.5 nm, where the abscissa is in units of Si reciprocal lattice unit in the hexagonal frame (rlu_h). The intense sharp peak centered at 6 rlu_h is the Si $(006)_h$, i.e., (222), reflection, and the broad peak centered at ~6.14 rlu_h, with its corresponding interplanar spacing close to d_{444} of cubic phase Y_2O_3, is attributed to the $(0012)_h$, i.e., (444), of Y_2O_3. Only the Y_2O_3 $(00l)_h$ reflections with l equal to 6 and 12 were observed on the radial scans along surface normal, evidencing the oxide films are (111) oriented. The position of Y_2O_3 $(0012)_h$ shifts monotonically to lower l values toward Si $(006)_h$, i.e., larger vertical lattice spacing, with increasing oxide thickness, which signifies the gradual relaxation of a laterally tensile-strained lattice in the thicker films. This is confirmed by the in-plane radial scans across Si $(110)_h$ surface reflection shown in the right panel of Fig. 1, where the broad Y_2O_3 peak progressively moved toward its bulk value, marked by the dashed line, with increasing thickness. Estimated from the FWHM of Y_2O_3 $(0012)_h$ reflections, the coherence length along the growth direction is always comparable to the film thickness, implying that the structural coherence extends over the whole film thickness. The presence of periodic Pendellosung fringes, which originate from the interference between the top and buried interfaces, reveals the atomically smooth interfaces and the high crystalline quality of the deposited layer.

The ω-rocking curves at Y_2O_3 $(0012)_h$ reflection are shown in the insets of Fig. 1. A small FWHM of 0.017° was obtained for a 3.6 nm thick film [slightly wider than the 0.008° FWHM of nearby Si $(006)_h$ reflection, which can be taken as the instrumentation limit]. Smaller peak width ~0.014° for thicker films has been observed. Moreover, we were able to measure a small FWHM of 0.033° from the 1.6 nm thick film. Such narrow rocking peak widths reveal excellent crystalline quality of the nanometer-thick oxide layers.

For thicker films, there exists an additional broad feature superimposed with the sharp peak. The broad component has a FWHM of 0.51° for 7.2 nm thick film. The width decreases to 0.44° when film thickness increases to 9.5 nm. We attribute the broad component to the misfit dislocations, which would introduce a pronounced mosaic broadening due to the strain field surrounding each dislocation. As the film is thin, e.g., 3.6 nm or thinner, the oxide layer is highly strained to the substrate with a lattice mismatch of ~0.9%, as revealed by the in-plane radial scans. In addition, no broad component was observed in the ω-rocking curve for these thin oxide films. With increasing layer thickness, e.g., 7.2 nm, the film structure gradually relaxes through the generation of dislocations, leading to the appearance of the broad component. With further thickness increasing to 9.5 nm, misfit dislocations and their strain fields would be gradually buried below and the width of mosaic spread gradually decreases. X-ray scattering results indicate that for Y_2O_3 films of thickness less than 10 nm, their crystal structure changes from a highly strained stage to a nearly fully relaxed one with increasing film thickness.

The FWHM of 0.017° in the ω-rocking scans for the 3.6 nm thick Y_2O_3 film is smaller than those of previously reported Y_2O_3 films with thickness exceeding 50 nm.[7] Furthermore, it is also smaller than those of Sc_2O_3 Ref. 10 and γ-Al_2O_3 Ref. 14 with similar oxide film thickness deposited using the UHV e-beam evaporation. This may be expected as the smaller lattice mismatch between Y_2O_3 and Si than those between Sc_2O_3 and γ-Al_2O_3 and Si.

In order to find the in-plane orientation relationship between Y_2O_3 and Si, azimuthal scans (ϕ scan) across Y_2O_3 $\{204\}_h$ centered around surface normal were performed. The intensity variation of a sample with 9.5 nm thick oxide layer is shown in Fig. 2. Two sets of sharp peaks with threefold symmetry were observed. The set with weaker intensity has the same in-plane orientation as Si $\{204\}_h$, i.e., $Y_2O_3[2\bar{1}\bar{1}]\|\text{Si}[2\bar{1}\bar{1}]$, known as *A*-type orientation and the stronger one (*B*-type orientation) is rotated 60° from the former one with $Y_2O_3[2\bar{1}\bar{1}]\|\text{Si}[11\bar{2}]$.[15] Linewidths of all six peaks are 0.06° or less, verifying a structural perfection and good in-plane alignment between the Y_2O_3 films and the Si (111) substrates. We also found that the ratio of the dominant *B*-type domain to the minor *A*-type domain grows with film thickness, implying that the *A*-type domain gets gradually buried upon further deposition. The fraction of *B*-type do-

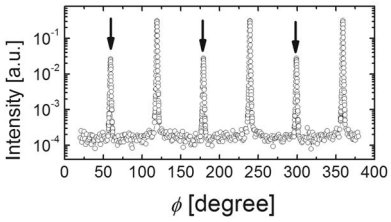

FIG. 2. ϕ cone scan over the family of cubic Y_2O_3 {400} reflections to confirm a threefold symmetry and the coexistence of A-B-type (111) domains. The arrows mark the angular positions of the Si {400} reflections, which coincide with the {400} reflections of minor A-type domain.

main exceeds 90% when film thickness is greater than ~5 nm.

Cubic phase Y_2O_3 has a lattice parameter about 2.4% smaller than twice that of Si, therefore, the in-plane lattice spacing of Y_2O_3 films pseudomorphically grown on Si (111) is expected to be tensile strained. Accordingly, the lattice along the growth direction would be compressed. The original cubic unit cell is then compressed along the body diagonal and undergoes a rhombohedral deformation.[16] The structure of the nanometer-thick oxide layer is, thus, more properly described as a pseudocubic structure. After verifying the crystal structure and orientation, we measured a series of Bragg reflections to determine the lattice parameters of the films. Over the range of film thickness investigated, 1.6–9.5 nm, we do observed a monotonic decrease/increase of lateral/normal lattice spacing. Up to 9.5 nm thick, the lattice of Y_2O_3 film is not fully relaxed yet; a lateral strain of ~0.4% still remains. For the thinnest film studied, 2 nm thick, the measured in-plane strain is ~1.6%, evidently less than the 2.4% expected for a fully strained layer.

Figure 3 shows a cross-sectional HR-TEM image of the Si/Y_2O_3 (7.2 nm)/Si (111) heterostructure along $[11\bar{2}]$ projection. The Y_2O_3/Si interface was found to be atomically sharp and smooth without any apparent interfacial layer, as previously reported.[7] To analyze the interfacial structure in more detail, a masking step and an inverse fast Fourier transform were applied to the fast Fourier transform of the original TEM image. Over the observed 18 nm length in the Fourier filtered image, we found misfit dislocations in the

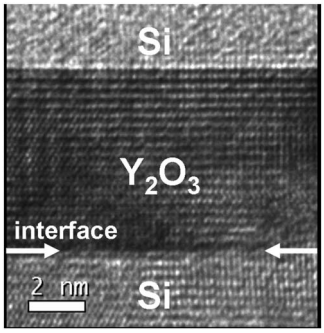

FIG. 3. A cross-sectional HR-TEM image of Y_2O_3/Si(111) heterostructure with film thickness of 7.2 nm in the $[11\bar{2}]$ projection.

oxide/Si interface, confirming the strain has been relaxed partially with the films thickness of 7.2 nm. However, regularly arranged misfit dislocations, as reported in the Sc_2O_3 films grown on Si (111),[10] were not observed here. The dynamic film growth condition and the early nucleation characteristics are potential causes to the absence of the regularly spaced dislocations in Fig. 3.

In conclusion, ultrathin Y_2O_3 epilayers were grown on Si (111) with excellent crystalline quality and atomically sharp, smooth oxide/Si interface. The attainment of very small rocking peak width of 0.014–0.017° in 7.2–3.6 nm thick oxide films, slightly wider than the instrumentation limit 0.008°, has now been achieved. This is perhaps the smallest width ever measured on nanometer-thick oxide films heteroepitaxially grown on Si. Please also note that Y_2O_3 1.6 nm thick (with only one and half lattice constant, ~6–7 bonding length of Y–O) was deposited and its excellent crystallographic characteristics were measured. The gradual lattice relaxation together with predominance of *B*-type domains with increasing thickness were observed for films less than 10 nm thick. The mechanism behind is currently under investigation.

The authors wish to thank the National Science Council, Taiwan for supporting this work. They would also like to thank the Center for Nano Science & Technology at NCTU, Taiwan for the help in the TEM.

[1] S. Guha, E. Cartier, M. A. Gribelyuk, N. A. Bojarczuk, and M. C. Copel, Appl. Phys. Lett. **77**, 2710 (2000), and the references therein.
[2] J. Kwo, M. Hong, A. R. Kortan, K. T. Queeney, Y. J. Chabal, J. P. Mannaerts, T. Boone, J. J. Krajewski, A. M. Sergent, and J. M. Rosamilia, Appl. Phys. Lett. **77**, 130 (2000).
[3] M. Hong, A. R. Kortan, H. M. Ng, J. Kwo, S. N. G. Chu, J. P. Mannaerts, A. Y. Cho, C. M. Lee, J. I. Chyi, and K. A. Anselm, J. Vac. Sci. Technol. B **20**, 1274 (2002).
[4] H. Ishiwara and T. Asano, Appl. Phys. Lett. **40**, 66 (1982).
[5] J. Kwo, M. Hong, A. R. Kortan, K. L. Queeney, Y. J. Chabal, R. L. Opila, Jr., D. A. Muller, S. N. G. Chu, B. J. Sapjeta, T. S. Lay, J. P. Mannaerts, T. Boone, H. W. Krautter, J. J. Krajewski, A. M. Sergnt, and J. M. Rosamilia, J. Appl. Phys. **89**, 3920 (2001).
[6] G. Apostolopoulos, G. Vellianitis, A. Dimoulas, M. Alexe, R. Scholz, M. Fanciulli, D. T. Dekadjevi, and C. Wiemer, Appl. Phys. Lett. **81**, 3549 (2002).
[7] M. H. Cho, D. H. Ko, Y. K. Choi, I. W. Lyo, K. Jeong, and C. N. Whang, Thin Solid Films **402**, 38 (2002), and references therein.
[8] M. E. Hunter, M. J. Reed, N. A. El-Masry, J. C. Roberts, and S. M. Bedair, Appl. Phys. Lett. **76**, 1935 (2000).
[9] M. Hong, J. P. Mannaerts, J. E. Bowers, J. Kwo, M. Passlack, W.-Y. Hwang, and L. W. Tu, J. Cryst. Growth **175-176**, 422 (1997).
[10] M. Hong, A. R. Kortan, P. Chang, Y. L. Huang, C. P. Chen, H. Y. Chou, H. Y. Lee, J. Kwo, M.-W. Chu, C. H. Chen, L. V. Goncharova, E. Garfunkel, and T. Gustafsson, Appl. Phys. Lett. **87**, 251902 (2005).
[11] C. H. Hsu, P. Chang, W. C. Lee, Z. K. Yang, Y. J. Lee, M. Hong, J. Kwo, C. M. Huang, and H. Y. Lee, Appl. Phys. Lett. **89**, 122907 (2006).
[12] Y. L. Huang, P. Chang, Z. K. Yang, Y. J. Lee, H. Y. Lee, H. J. Liu, J. Kwo, J. P. Mannaerts, and M. Hong, Appl. Phys. Lett. **86**, 191905 (2005).
[13] P. A. Bennett, M. Y. Lee, P. Yang, R. Schuster, P. J. Eng, and I. K. Robinson, Phys. Rev. Lett. **75**, 2726 (1995).
[14] S. Y. Wu, M. Hong, A. R. Kortan, J. Kwo, J. P. Mannaerts, W. C. Lee, and Y. L. Huang, Appl. Phys. Lett. **87**, 091908 (2005).
[15] R. T. Tung and J. L. Batstone, Appl. Phys. Lett. **52**, 1611 (1988).
[16] M. Friak, A. Schindlmayr, and M. Scheffler, New J. Phys. **9**, 5 (2007).